



ORIGINAL RESEARCH ARTICLE

# Microstructures and Properties of WC-10 wt.%CoCrFeNiAl<sub>x</sub> Composite Cemented Carbides

Wenkai Zhao, Zhiping Sun, Zhiming Wang, Zhiwei Shang, and Yaning Chen

Submitted: 18 July 2023 / Revised: 9 January 2024 / Accepted: 10 February 2024

In this paper, WC-10 wt.%CoCrFeNiAl<sub>x</sub> cemented carbide was prepared by a vacuum pressureless tube furnace using the high-entropy alloy CoCrFeNiAl<sub>x</sub> ( $x = 0, 0.25, 0.5, 0.75, 1.0$ ) as the binder phase. The effects of Al content changes on the microstructures and mechanical properties of cemented carbides were analyzed. The results showed that the high-entropy alloy as the binder phase could significantly refine the grain size of WC and enhance its mechanical properties. With increasing Al content, the densification of cemented carbide decreased gradually, but the hardness increased gradually; moreover, the fracture toughness and flexural strength appeared to first increase and then decrease. When the Al content was  $x = 1.0$ , the densification was the lowest, but the hardness reached a maximum value of 1898.5 MPa, and the fracture toughness and flexural strength reached relatively low values of 7.76 MPa m<sup>1/2</sup> and 680 MPa, respectively. When the Al content was  $x = 0.25$ , the hardness value reached 1822.4 MPa, and the fracture toughness and flexural strength reached 10.72 MPa m<sup>1/2</sup> and 1350 MPa, respectively; this composite exhibited optimal overall performance and had the potential to replace Co as a new binder phase.

**Keywords** cemented carbide, high-entropy alloy binder phase, microstructure, mechanical properties

## 1. Introduction

Cemented carbides, also known as cermets, can be prepared by using ceramics or hard equivalent refractory metal compounds as the matrix and transition metals (Co, Cr, Fe, etc.) as the binder phase (Ref 1, 2). A hard phase with a good modulus of elasticity is the framework of an alloy that provides good hardness, and the ductile bonding phase acts as an adhesive that promotes sintering densification and provides good toughness (Ref 3, 4). WC-Co cemented carbide has the advantages of high hardness, good strength, wear resistance and corrosion resistance, and it is widely used in industrial fields to date. However, Co is a strategic resource, that is expensive and toxic, and long-term exposure increases the risk of cancer. The search for new bonding phases to replace Co with excellent properties is a popular topic in the field of cemented carbides (Ref 5, 6).

A high-entropy alloy (HEA) is a multicomponent alloy system with at least five principal elements, where each element accounts for approximately 5-35 at.% of the total system, and the atomic radius differences among them are not significant. According to conventional wisdom, multicomponent alloy

systems tend to form intermetallic compounds, which can affect their mechanical properties (Ref 7, 8). However, HEAs usually form only a simple solid solution due to the strong mutual solid solution ability of the group elements, and their excellent properties of high strength, high toughness, high temperature resistance, and corrosion resistance give them the potential to replace Co as the bonding phase of cemented carbide. In addition, the interactions and radius differences between different atoms of HEAs produce lattice distortions and slow diffusion effects, which impede the dissolution and diffusion of WC in liquid-phase HEAs; furthermore, grain refinement can be achieved without adding inhibitors, which is conducive to obtaining carbide alloys with improved overall performance (Ref 9-11).

In recent years, a number of studies have demonstrated that HEAs can feasibly serve as binder phases for WC-based cemented carbides. Zhu et al. (Ref 9) prepared WC-HEA cemented carbide by SPS using the high-entropy alloy CoCrFeNiAl as the binder phase and studied the microstructures and properties of cemented carbide with different binder phase contents and temperatures. The results showed that increasing the sintering temperature can promote the phase transition of HEA from BCC-FCC; additionally, for the composite material, the hardness decreases, the fracture toughness increases, and the comprehensive mechanical properties are optimal when the content of HEA is 10 wt.%. Zhou et al. (Ref 12) prepared ultrafine-grained WC-AlFeCoNiCrTi and WC-Co cemented carbides by hot-press sintering under the same process parameters and studied their microstructures and mechanical properties. The results showed that the high-entropy alloy can obviously inhibit the growth of WC grains, and its mechanical and corrosion resistance properties are better than those of WC-Co. Chen et al. (Ref 13) prepared a WC-based cemented carbide with a single FCC-phase-structured

Wenkai Zhao, Zhiping Sun, Zhiming Wang, Zhiwei Shang, and Yaning Chen, School of Mechanical Engineering, Qilu University of Technology (Shandong Academy of Sciences), Jinan 250353, China; and Shandong Institute of Mechanical Design and Research, Jinan 250353, China. Contact e-mail: sunzp4259@qlu.edu.cn.

high-entropy alloy  $\text{Al}_{0.5}\text{CoCrCuFeNi}$  as the binder phase and found that the WC grains are homogeneously dispersed in the polyalloy without the formation of a second phase, and their grain sizes are significantly smaller than those in WC-Co. The hardness is higher than that of WC-Co at both room and elevated temperatures, and the fracture toughness of WC-20 wt.% $\text{Al}_{0.5}\text{CoCrCuFeNi}$  cemented carbide reaches  $17.4 \text{ MPa m}^{1/2}$ , which is 30% higher than that of the commercial WC-Co at the same hardness; additionally, the microhardness and abrasion resistance decrease dramatically as the content of the bonding phase increases. These studies show that HEA as a binder phase contributes to the excellent mechanical properties of WC cemented carbides, but their relationship lacks in-depth study. It has been shown (Ref 14, 15) that the element Al has a larger atomic radius than other elements and that the microstructures and properties of high-entropy alloys can be significantly altered by changing the content of Al. However, few studies have been conducted on the application of Al to WC cemented carbide, and the results are still unclear.

In this study, WC-10 wt.%  $\text{CoCrFeNiAl}_x$  cemented carbide was prepared by conventional vacuum sintering using a high-entropy alloy  $\text{CoCrFeNiAl}_x$  system instead of Co as the binder phase and WC as the hard phase, as an extension of previous work (Ref 9), to investigate the properties and the effects of variation in the elemental content of Al in the binder phase on the microstructure and mechanical properties of cemented carbide.

## 2. Experimental details

### 2.1 Material Preparation

Co, Cr, Fe, Ni, and Al powder (>99.9% purity,  $d_{50} = 50 \mu\text{m}$ , Nanjing Xindun Alloy Materials Co., Ltd., China) were used to produce  $\text{CoCrFeNiAl}_x$  high-entropy alloys and commercial WC powder (> 99.9% purity,  $d_{50} = 1.95 \mu\text{m}$ , Vilory Advanced Material Co., Ltd., China) was selected to prepare WC-10 wt.% $\text{CoCrFeNiAl}_x$  ( $x = 0, 0.25, 0.5, 0.75, 1$ ) mixed powders. The five mixed powders were placed in a ball milling jar; the ball milling medium was YG6 ball, the ball material ratio was 10:1, and the rotational speed was 300 r/min. Then, 40 g of alcohol (> 99.5% purity, Jinan Chaoxu Instrument Co., Ltd.) was added to each ball milling jar as a control agent for the wet grinding process. The powder was mixed and milled using a high-energy planetary ball mill for 36 h, after which the powder was dried in a vacuum drying oven at  $80 \text{ }^\circ\text{C}$  for 12 h and passed through a 100 mesh sieve.

### 2.2 Sintering

Circular samples with a diameter of 30 mm and height of 6 mm were prepared by taking 25 g of mixed powder and holding it under a uniaxial pressure of 200 MPa in a hydraulic press for 30 s. Afterward, the samples were placed in a tube furnace to be heated to  $1450 \text{ }^\circ\text{C}$ , held for 60 min and then, cooled to room temperature (heating and cooling rate of  $5 \text{ }^\circ\text{C}/\text{min}$ ). To avoid oxidization of the samples during sintering, titanium powder was placed separately in the furnace tube to absorb excess oxygen, while argon gas was continuously charged throughout for protection (Ref 16).

## 2.3 Sample Characterization

X-ray diffraction (XRD) analyses of the pre-sintered powder and the sintered samples were performed using an x-ray diffractometer (BRUKER D2 PHASER RAX-30). The operating voltage was 40 V, and the operating current was 200 mA. The scanning step size was  $0.026^\circ$ , and the scanning angle range was from  $10^\circ$  to  $90^\circ$ . Scanning electron microscopy (SEM) in backscattered electron (BSE) mode and energy-dispersive x-ray spectroscopy (EDS) techniques were used to analyze the microstructures and elemental compositions of the pre-sintered powder and the sintered samples. The WC grain size and distribution were statistically analyzed using the line intercept method, with at least 200 grains being analyzed for each sample. The density of the alloy was determined using the Archimedes drainage method. The hardness of the alloy was measured using a Vickers hardness tester (HVS-30) under a 30 kg load for 15 seconds. The fracture toughness of the samples was calculated using the length of the indentation crack, with the following formula (Ref 17, 18):

$$K_{IC} = 0.15 \times \sqrt{HV_{30} / \sum_{i=1}^4 l_i} \quad (\text{Eq 1})$$

where  $HV_{30}$  (kgf  $\text{mm}^{-2}$ ) is the Vickers hardness value, and  $l_i$  is the crack length (mm) observed under a Leica microscope at  $500\times$  magnification. The samples were cut into standard specimens with dimensions of  $20 \text{ mm} \times 4 \text{ mm} \times 3 \text{ mm}$  and polished to a surface roughness of less than  $0.1 \mu\text{m}$ . The flexural strength of the alloy was determined using a universal testing machine (AGS-X5KN) through a three-point bending test. The loading rate was set at  $0.5 \text{ mm}/\text{min}$ , and the span between the support points was set at 14 mm. The formula for calculating the flexural strength  $\sigma$  was as follows (Ref 19):

$$\sigma = 3PL/2bh^2 \quad (\text{Eq 2})$$

where  $P$  is the load (N) at the fracture of the alloy,  $L$  (mm) is the span between the support points, and  $b$  and  $h$  are the width and height (mm) of the specimen, respectively. To ensure data accuracy, all mechanical property experimental data in this study were reported as the average of 6-8 experimental results.

## 3. Results and Discussion

### 3.1 Powder Characterization

The SEM images in Fig. 1(a) and (b) depict the initial WC powder and the ball-milled WC-10 wt.% $\text{CoCrFeNiAl}_{0.5}$  composite powder, respectively. The initial WC powder exhibited mostly spherical shapes, while after 36 hours of ball milling with HEA powders, the shape and particle size underwent significant changes. Larger spherical particles were broken down into smaller and more irregular shapes than before. Due to the reduced particle size after ball milling, the powders tended to aggregate and form relatively large powder particles.

The components of HEA powder and WC-HEA mixed powder after ball milling are shown in Tables 1 and 2. The content of carbon and oxygen in the powder after ball milling is normal, which also indicates that the powder was not contaminated during the ball milling process.

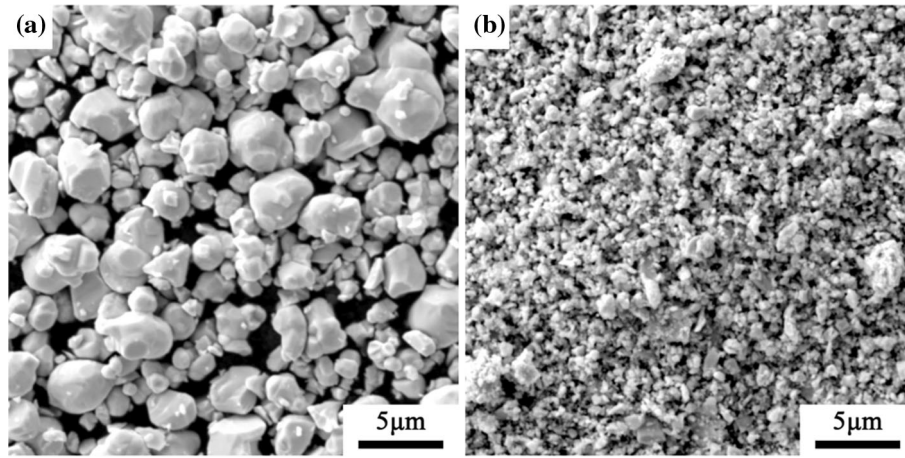


**Fig. 1** (a) SEM image of the initial WC powder and (b) SEM image of the ball-milled WC-10 wt.%CoCrFeNiAl<sub>0.5</sub> composite powder

**Table 1** Contents of ball-milled CoCrFeNiAl<sub>x</sub> powder (wt.%)

Elements	Co	Cr	Fe	Ni	Al	O
$X = 0$	26.17	22.96	24.86	25.92	0	0.09
$X = 0.25$	25.29	22.28	24.25	25.23	2.91	0.04
$X = 0.5$	24.55	21.62	23.70	24.47	5.64	0.02
$X = 0.75$	23.89	21.04	22.97	23.78	8.27	0.05
$X = 1.0$	23.18	20.46	22.15	23.47	10.68	0.06

**Table 2** Contents of ball-milled WC-HEA composite powder (wt.%)

Elements	W	C	O	Co	Cr	Fe	Ni	Al
$X = 0$	86.62	2.41	< 0.01	2.94	2.45	2.75	2.82	0
$X = 0.25$	85.71	3.44	< 0.01	2.83	2.53	2.61	2.55	0.32
$X = 0.5$	85.73	3.75	< 0.01	2.81	2.47	2.63	2.09	0.51
$X = 0.75$	86.00	4.26	< 0.01	2.58	2.47	2.62	1.29	0.77
$X = 1.0$	85.88	3.98	< 0.01	2.62	1.73	2.43	2.58	0.78

Figure 2 shows the XRD pattern of the mechanically alloyed high-entropy alloy powder. When the content of Al is  $x = 0$ , the main phase of the FCC phase and the secondary phase of the BCC phase are detected in the high-entropy alloy powder, and with the increase in the content of Al, the FCC phase gradually changes to the BCC phase. When the content of Al is  $x = 1.0$ , only the BCC phase is detected in the phase structure. This phenomenon is attributed to the fact that the atomic packing density of the BCC structure is lower than that of the FCC structure, and the lattice constant of the alloy increases with increasing aluminum content, resulting in the loss of stability of the originally tightly packed FCC structure and the formation of a looser BCC phase (Ref 20). Figure 3 shows the XRD pattern of the ball-mused WC-HEA composite powder. Compared with the original WC powder, due to grain thinning and strain generation, the diffraction peak of the ball-mused WC composite powder becomes shorter and wider. Furthermore, the

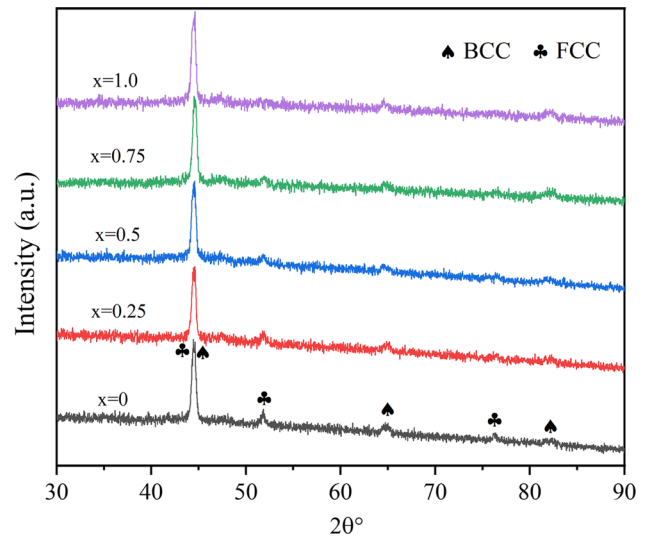


**Fig. 2** XRD pattern of CoCrFeNiAl<sub>x</sub> ( $x = 0, 0.25, 0.5, 0.75, 1.0$ ) powder

phases of the HEA binders remain unchanged during the ball mill mixing process.

### 3.2 Microstructural Analysis of the WC-HEA Cemented Carbide

Figure 4 shows the SEM images of WC-10 wt.%Co and five kinds of WC-HEA cemented carbides prepared under the same process parameters. Combined with the element distribution and XRD pattern in Fig. 5, the white part in the figure is the hard phase of WC, and the gray part and black dots distributed around WC are the Co or HEA-bonded phase. The surface morphologies of WC-Co and WC-HEA are very different. In WC-Co, the WC grains are more irregular and larger in size, while in WC-HEA, the WC grains become more regular and smaller in size. With increasing Al content, the number of black dots on the surface increases, and there is additional precipitation on the polished surface. EDS point scanning analysis is performed on the black region in the figure, and the results are shown in Table 3. Relative to other elements, the content of O

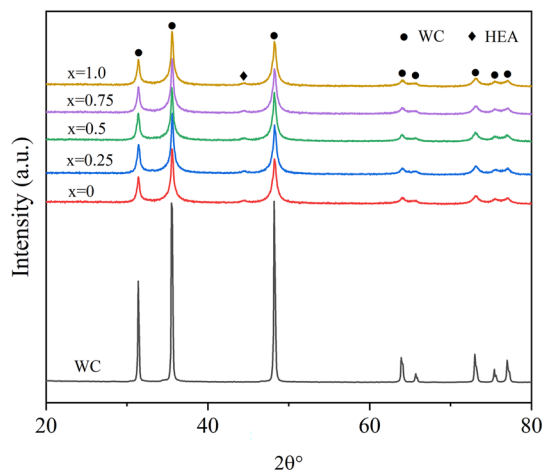


**Fig. 3** XRD pattern of the initial WC powder and WC-HEA cemented carbide composite powder after ball milling

is higher in the black region, and Al and Cr have higher affinities for O. These regions may exhibit these phenomena due to the oxide compositions of Al and Cr.

Figure 5 shows that although there are differences in the distributions of Co, Cr, Fe, Ni and Al, the five elements are basically evenly distributed in the sample, and no precipitation similar to intermetallic compounds occurs. In addition, the formation of pores is related to the enrichment of high-melting point elements, such as Co, Cr, Fe and Ni, among which Cr and Ni are the most obvious. In the liquid-phase sintering process, HEA melts into liquid and diffuses into the cracks of WC grains under the action of surface tension, and the bonded phase shrinks in the melting state, thus producing pores (Ref 21, 22). Compared with other elements, Al has a lower melting point, and sublimation occurs during the liquid-phase sintering process and enters the pores, resulting in its near absence in the gray bonding phase.

The average grain size of WC in WC-Co is 1.27  $\mu\text{m}$ , while in WC-HEA, the average grain sizes of WC are 1.04, 0.85, 0.88, 0.98, and 1.02  $\mu\text{m}$ , as shown in Fig. 4(b)-(f), respectively. The growth of WC grains in WC-HEA occurs through the process of dissolution-precipitation-recrystallization (Ref 23). When the temperature exceeds 1400  $^{\circ}\text{C}$ , WC grains dissolve in the liquid Co or HEA binder phase, followed by diffusion into the interior of the binder phase. The solubility of WC grains decreases as the temperature decreases, leading to the precipitation of WC grains at the edges of larger WC grains and resulting in grain growth by recrystallization. Due to the different binder phases, there are differences in the solubility and diffusion capabilities of WC. The HEA, with a high number of elements, exhibits lattice distortion and slow diffusion effects due to the interactions and radius differences between the elements, which hinder the dissolution and diffusion of WC, leading to relatively small and rounded WC grains. The HEA not only inhibits the growth of WC grains during sintering but also shows a close correlation with the Al content. Figure 6 shows the microstructure evolution of cemented carbide with different Al content; among the five elements (Co, Cr, Fe, Ni, and Al), Al has the largest atomic radius. The addition of Al increases the atomic size difference in the HEA, resulting in significant lattice distortion and

influencing the atomic diffusion rate, the average grain size of WC decreases. However, when the content of Al is further increased, the content of Ni with the slowest diffusion rate is reduced (Ref 24), which weakens its hysteretic diffusion effect, resulting in the grain size of WC gradually increasing; however, it is still smaller than that in WC-Co.

### 3.3 Phase Analysis of WC-HEA Cemented Carbides

Figure 7 shows the XRD pattern of the WC-10 wt.%CoCr-FeNiAl<sub>x</sub> cemented carbide after sintering. Compared with the mixed powder of WC-HEA before sintering, the diffraction peak of WC-HEA after sintering becomes narrower, but the strength increases due to the increase in the grain size and the release of microstrain. In addition, some diffraction peaks of  $\eta$ -carbides (Co, Fe, Ni)<sub>3</sub>W<sub>3</sub>C appear. The face-centered cubic structure ( $a = b = c = 11.1118 \text{ \AA}$ ) of (Co, Fe, Ni)<sub>3</sub>W<sub>3</sub>C typically appears during liquid-phase sintering of WC and metal alloys (Ref 10). Moreover, in the solid-state sintering process, slow diffusion of free carbon leads to the localized decarburization of the cemented carbide and promotes the formation of  $\eta$ -carbide. The diffraction peak related to WC is clearly visible; the diffraction peak of high-entropy alloy is very weak; on the one hand, because the content of high-entropy alloy itself is small; on the other hand, the vast majority of high-entropy alloys react with WC to form intermetallic compounds. However, the major phases of the HEA binders with different Al contents transform into FCC. This transformation indicates that high temperatures during sintering accelerate the transformation of HEA from BCC to FCC, and the FCC phase can be stable at a high temperature for CoCrFeNiAl<sub>x</sub> high-entropy alloys.

### 3.4 Relative Density of WC-HEA Cemented Carbides

Relative density is an important index to reflect the internal defects of materials and has a certain impact on mechanical properties. Figure 8 shows the relative density of the WC-HEA cemented carbide. The figure shows that when the Al content  $x = 0$ , it has the highest relative density (97.5%). With the gradual increase in Al, the relative density of the material gradually decreases. When the Al content is  $x = 1.0$ , the relative density is the lowest (95%). The relative density of the sintered material is affected by many factors, including the type of bonding phase, sintering method, sintering temperature and holding time (Ref 25-27). Under the same sintering process parameters, Co exhibits the best wettability on WC, with a contact angle of approximately  $0^{\circ}$ . However, the presence of multiple principal elements in HEA leads to a decrease in wetting ability with WC. Previous studies have shown (Ref 28) that the introduction of Al can result in a slower wetting rate and decreased wetting ability, which is consistent with the findings of this study regarding the gradual decrease in relative density with increasing Al content.

### 3.5 Hardness of WC-HEA Cemented Carbides

Figure 9 shows the hardness of the WC-HEA cemented carbide. The figure shows that adding a small amount of Al can significantly improve the hardness of cemented carbide. However, with the further increase in Al content, the grain size gradually increases, and the relative density gradually decreases, resulting in a gradual decrease in hardness. When the relative density is low and the grain size is large, the hardness

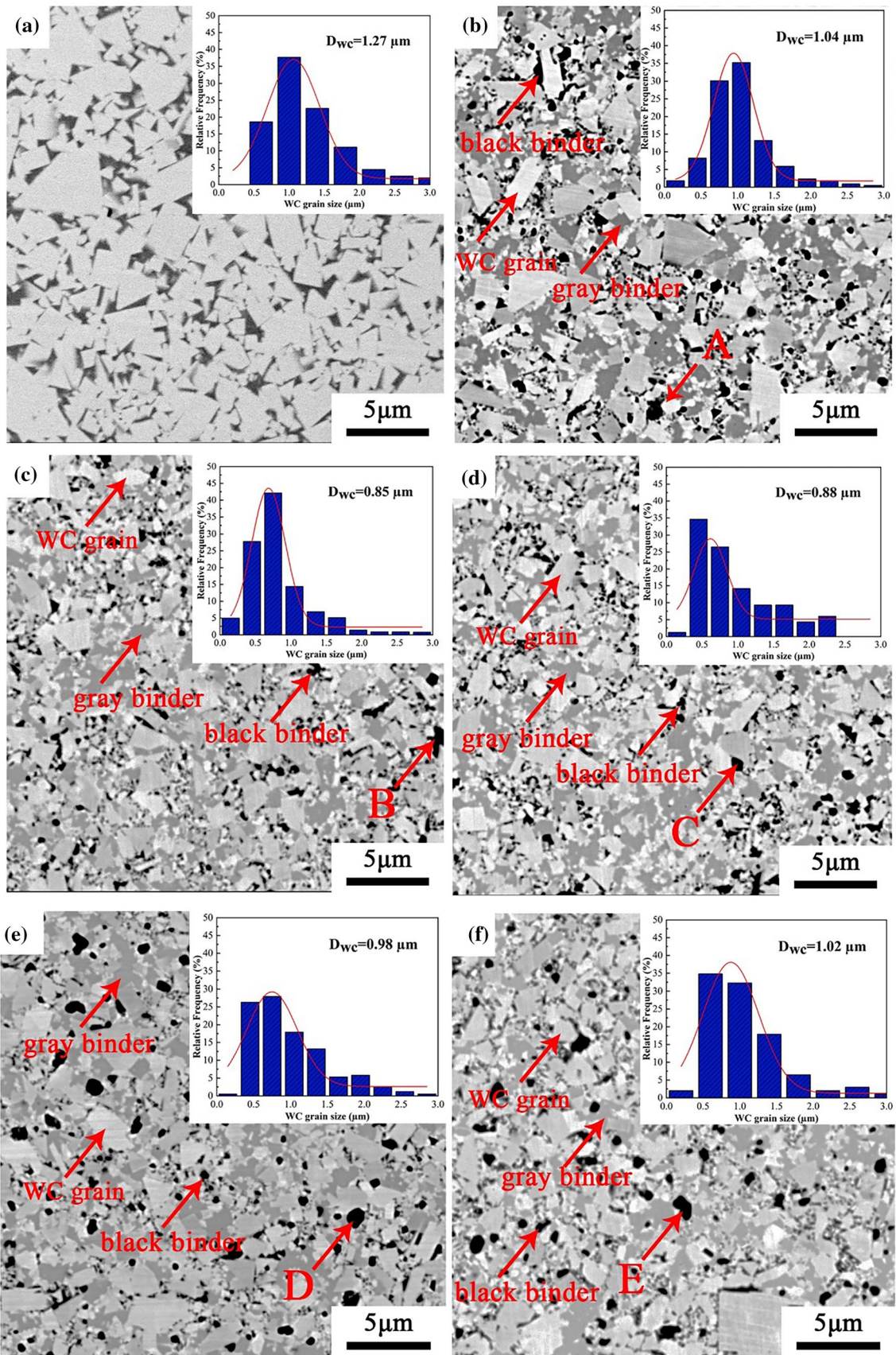
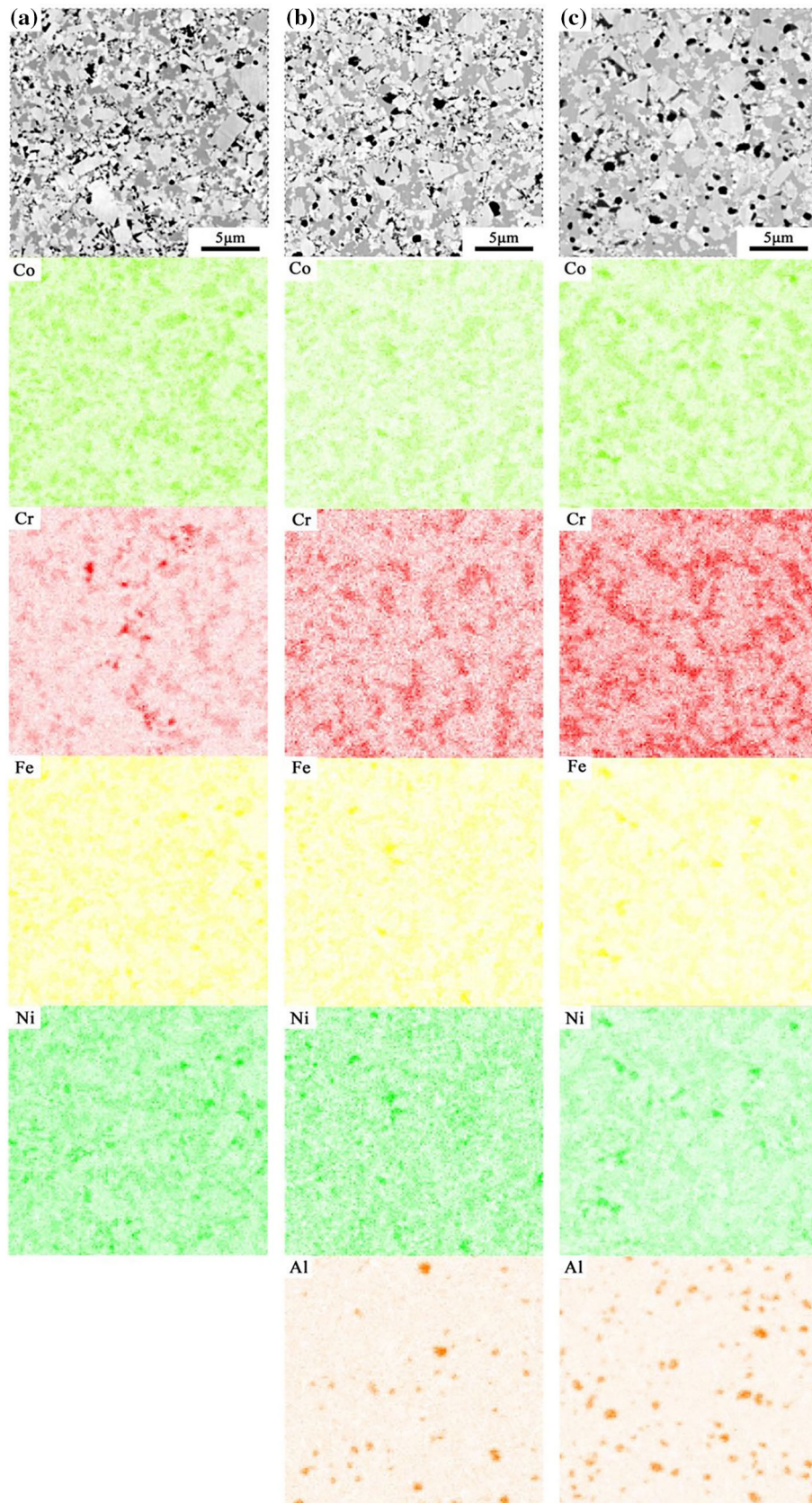


Fig. 4 Microstructure and WC grain size distribution of WC-10 wt.%Co and WC-10 wt.%CoCrFeNiAl<sub>x</sub> cemented carbides: (a) WC-10 wt.%Co; (b)  $x = 0$ ; (c)  $x = 0.25$ ; (d)  $x = 0.5$ ; (e)  $x = 0.75$ ; and (f)  $x = 1.0$



**Fig. 5** Elemental distribution in WC-10 wt.%CoCrFeNiAl<sub>x</sub> cemented carbides: (a)  $x = 0$ ; (b)  $x = 0.5$ ; and (c)  $x = 1.0$

**Table 3** Elemental analysis (at.%) of different regions using EDS

Elements	W	C	O	Co	Cr	Fe	Ni	Al
A	14.46	...	16.72	8.78	36.33	7.10	14.63	...
B	25.03	...	16.31	5.13	15.10	4.28	10.89	23.26
C	21.01	...	34.64	...	14.28	...	...	30.07
D	32.01	...	30.70	3.25	8.76	1.36	4.28	19.64
E	40.23	...	20.36	7.23	11.42	2.47	3.56	14.73

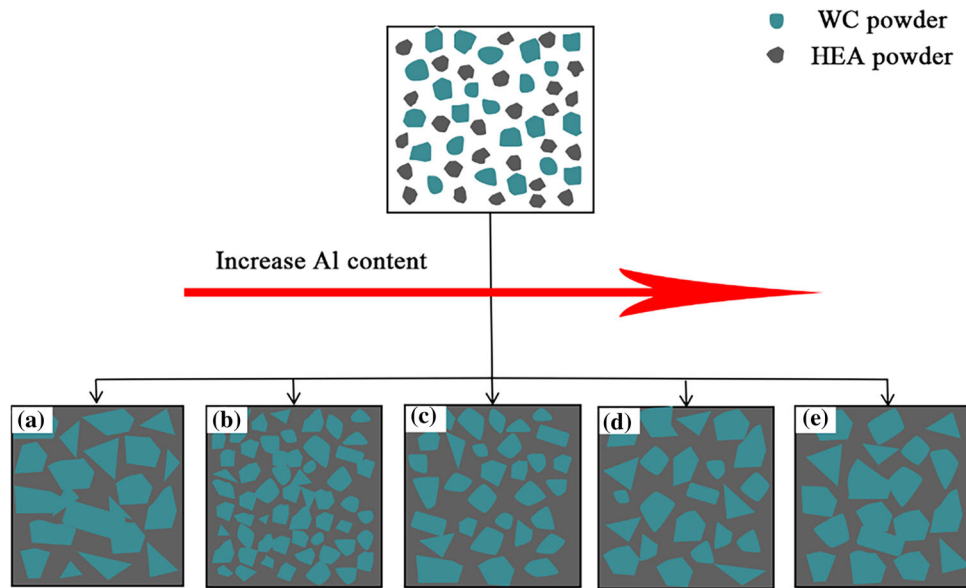


**Fig. 6** Schematic representation of the morphology evolution of WC-10%CoCrFeNiAl<sub>x</sub> cemented carbides: (a)  $x = 0$ ; (b)  $x = 0.25$ ; (c)  $x = 0.5$ ; (d)  $x = 0.75$ ; and (e)  $x = 1.0$

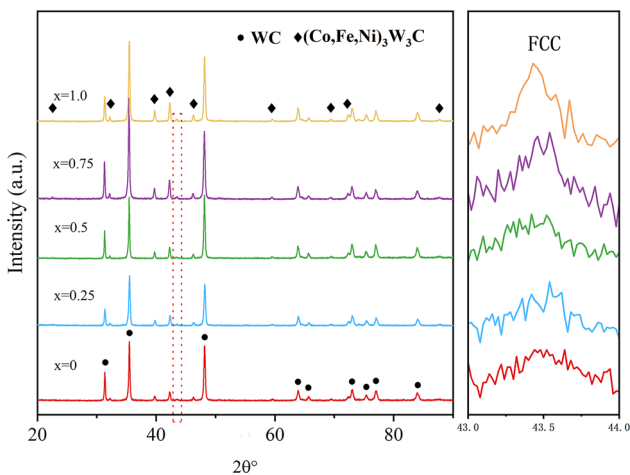


**Fig. 7** XRD spectrum of the sintered WC-10 wt.%CoCrFeNiAl<sub>x</sub> cemented carbide

value reaches the highest value of 1898.5 MPa. According to the Hall–Petch equation (Ref 29) and the relationship between yield strength and hardness (Ref 30), the smaller the grain size is, the more significant the grain boundary strengthening effect and the more obvious the hardness improvement. When the content of Al is  $x = 1.0$ , the grain size is larger, but the hardness is the highest. The reason for this phenomenon should be

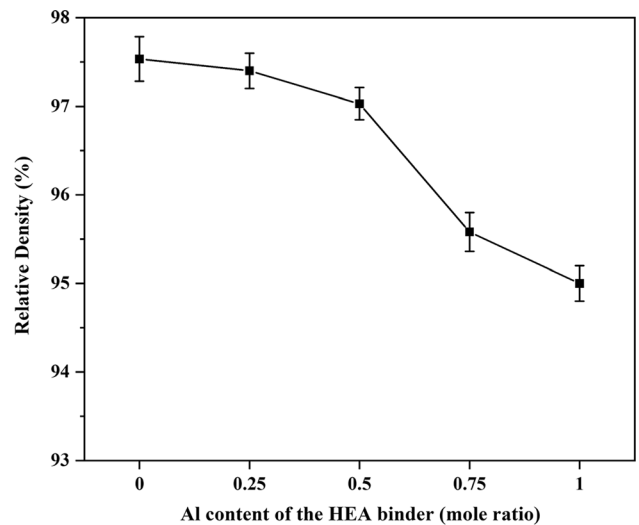


**Fig. 8** Relative densities of WC-10 wt.%CoCrFeNiAl<sub>x</sub> cemented carbides

attributed to the increase in Al content in the HEA binder phase, which leads to an increase in the atomic size difference  $\delta$  and the more serious lattice distortion (Ref 31). This phenomenon leads to increases in the Young's modulus and lattice strain effect in the HEA bonding phase, which increases the

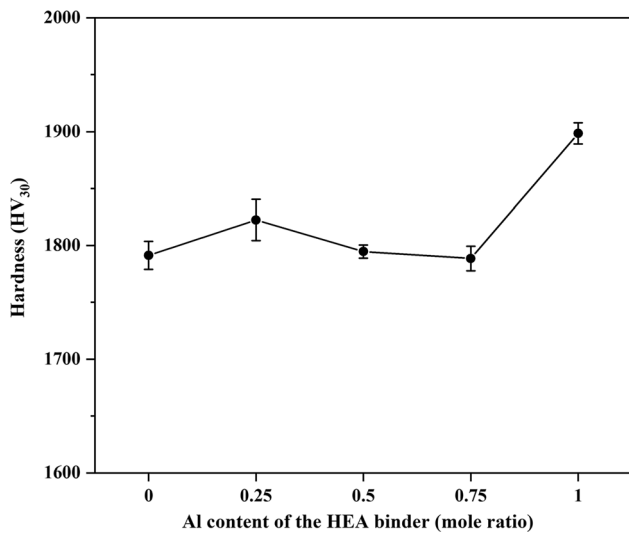


**Fig. 9** Hardnesses of WC-10 wt.%CoCrFeNiAl<sub>x</sub> cemented carbides

hardness of the HEA bonding phase (Ref 32) and thereby the hardness of the WC-HEA cemented carbide. In addition, studies have shown (Ref 24, 33) that with increasing Al content, the adjacency in WC-HEA cemented carbide increases, and a high adjacency suggests that the WC/WC contact has a relatively high stiffness, which contributes to the improvement in hardness.

### 3.6 Fracture Toughness of WC-HEA Cemented Carbides

Figure 10 shows the fracture toughness diagram of the WC-CoCrFeNiAl<sub>x</sub> cemented carbides. With an increase in Al content, the fracture toughness exhibits a trend of first increasing and then decreasing. The maximum fracture toughness value of 10.72 MPa m<sup>1/2</sup> is achieved at an Al content of  $x = 0.25$ . Subsequently, the fracture toughness gradually decreases with a further increase in the Al content. The fracture toughness of WC-HEA cemented carbides is influenced by factors such as density, wettability between HEA and WC, sintering characteristics of the binder phase, and deformation ability. The high-entropy alloy exhibits good deformation ability, which enhances the fracture toughness of the cemented carbides as a binder phase. However, excessively high Al content leads to lower density and larger grain size, directly affecting the fracture toughness. At an Al content of  $x = 1.0$ , the fracture toughness value is only 7.76 MPa m<sup>1/2</sup>. Figure 11 shows the SEM morphologies of indentation cracks in the cemented carbides. Due to the higher hardness of the HEA binder phase, when the crack reaches the binder phase, it forms a sawtooth pattern, hindering crack propagation and causing crack deflection (Ref 34, 35). From the figure, it can be observed that when the binder phase is reduced to a point, the bridging material is pulled out of the matrix, hindering further crack propagation behind the crack, leading to the occurrence of crack bridging (Ref 36). Further observation reveals that in the critical region between the WC grains and the binder phase, some WC grains are pulled out, which is an energy-consuming mechanism. Additionally, the smaller the WC grain size is, the more grain boundaries are generated, resulting in higher energy consumption during crack propagation. These phenomena

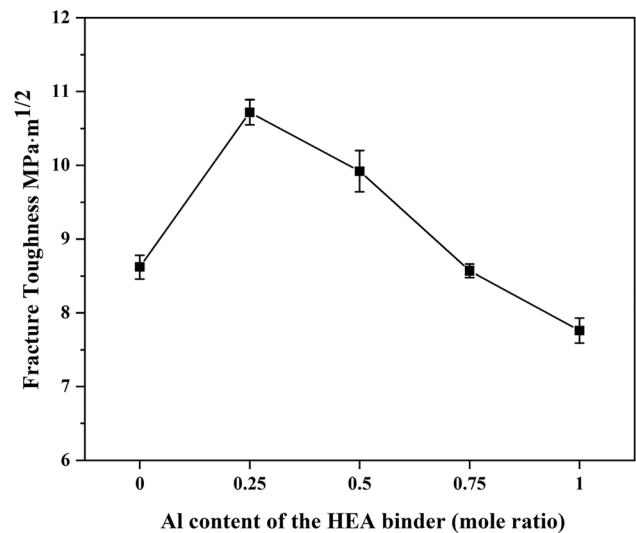


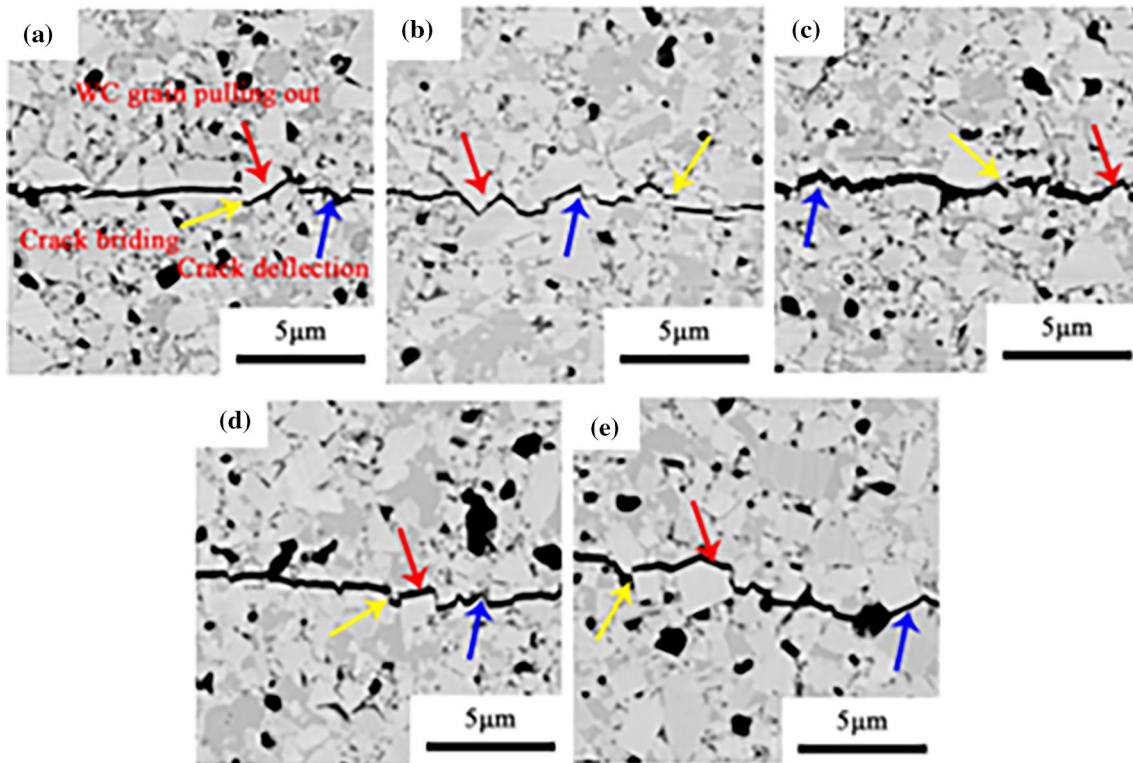
**Fig. 10** Fracture toughnesses of WC-10 wt.%CoCrFeNiAl<sub>x</sub> cemented carbides

collectively contribute to the enhancement of fracture toughness in cemented carbides when HEAs are used as the binder phase.

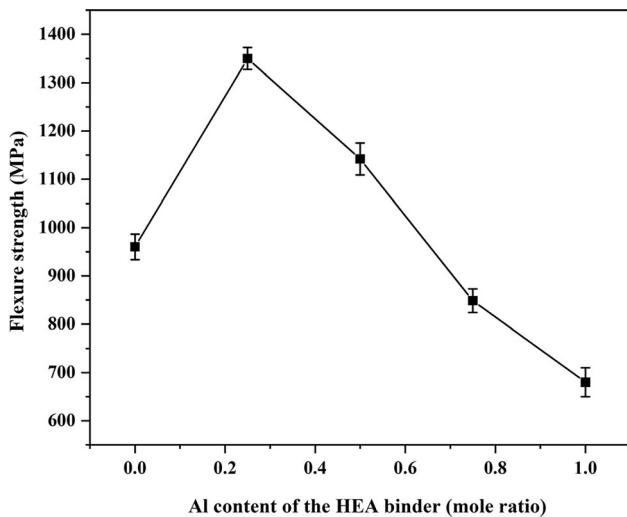
### 3.7 Flexural Strength of WC-HEA Cemented Carbides

Figure 12 shows the flexural strengths of WC-10 wt.%CoCrFeNiAl<sub>x</sub> cemented carbides with different Al contents. The graph shows that the flexural strength of the alloy first increases and then decreases with increasing Al content. The alloy exhibits the highest flexural strength of 1350 MPa at an Al content of  $x = 0.25$ . Subsequently, the flexural strength decreases significantly as the Al content further increases, reaching a value of 680 MPa at an Al content of  $x = 1.0$ . The flexural strength of WC-HEA cemented carbides is mainly influenced by factors such as WC grain size, composition and content of the binder phase, microstructure, and porosity. Figure 13 presents the fracture surface morphologies of the cemented carbides with different Al contents. The addition of Al induces lattice distortion and refinement of the WC grain size. An abundance of grain boundaries imposes additional resistance to the movement and formation of dislocations, making the material more difficult to deform. This effect requires the alloy to consume additional energy during fracture, resulting in better flexural strength than alloys without added Al. The fracture surface morphology reveals predominantly transgranular fracture in WC-HEA cemented carbides with varying Al contents, along with some intergranular fracture and dimple fracture (Ref 34, 37). Transgranular fracture mainly occurs at large WC grains, and theoretically, an increase in Al content leads to further transgranular fractures. Transgranular fracture requires overcoming high-energy barriers, indicating increased flexural strength. However, the flexural strength decreases as the Al content increases from  $x = 0.25$  to  $x = 1.0$ . This decrease is attributed to the significant influence of porosity, which causes stress concentration and nucleation of cracks during deformation. Increasing the Al content reduces the wettability between the HEA binder phase and WC, leading to decreased densification and increased porosity in sintered





**Fig. 11** SEM images of the indentation crack morphology of WC-10 wt.%CoCrFeNiAl<sub>x</sub> cemented carbides: (a)  $x = 0$ ; (b)  $x = 0.25$ ; (c)  $x = 0.5$ ; (d)  $x = 0.75$ ; and (e)  $x = 1.0$



**Fig. 12** Flexural strengths of WC-10 wt.%CoCrFeNiAl<sub>x</sub> cemented carbides

samples and thereby reducing the flexural strength of the alloy. Therefore, the optimum flexural strength is achieved when the Al content is  $x = 0.25$ .

## 4. Conclusions

The WC-10 wt.%CoCrFeNiAl<sub>x</sub> ( $x = 0, 0.25, 0.5, 0.75, 1.0$ ) cemented carbides were produced by pressureless sintering and then the effects of Al element content on microstructures and

mechanical properties were studied. Based on the above results and discussion, the following conclusions were obtained:

- (1) Due to the slow diffusion effect of high-entropy alloy, with HEAs as the binder phase, the grain size of WC is obviously refined. In addition, reducing the content of Al can enhance the inhibition effect of high-entropy alloy on the growth of WC grains, which leads to a fine microstructure.
- (2) Tungsten carbide with HEAs as the binder phase is not as dense as WC-Co, but its hardness is increased by 58%. In addition, with increasing Al content, the hardness as a whole shows an upward trend.
- (3) With increasing Al content, the fracture toughness and bending strength of cemented carbide first increase and then decrease. When the Al content is  $x = 0.25$ , the fracture toughness and bending strength of cemented carbide are the best, reaching  $10.72 \text{ MPa m}^{1/2}$  and 1350 MPa, respectively. The toughening mechanisms of fracture toughness are grain pulling out, crack deflection and crack bridging. Theoretically, with increasing Al content and increasing WC grain size, additional transgranular fractures occur, and the bending strength increases. In fact, the decrease in density caused by excessive Al content plays a dominant role in its bending strength, and the bending strength decreases.

Therefore, using high-entropy alloys as the bonding phase can significantly refine the grain size of WC and enhance its mechanical properties. When the content of Al element is relatively low, its overall performance is optimal, demonstrating the potential to replace Co as a new type of bonding phase.

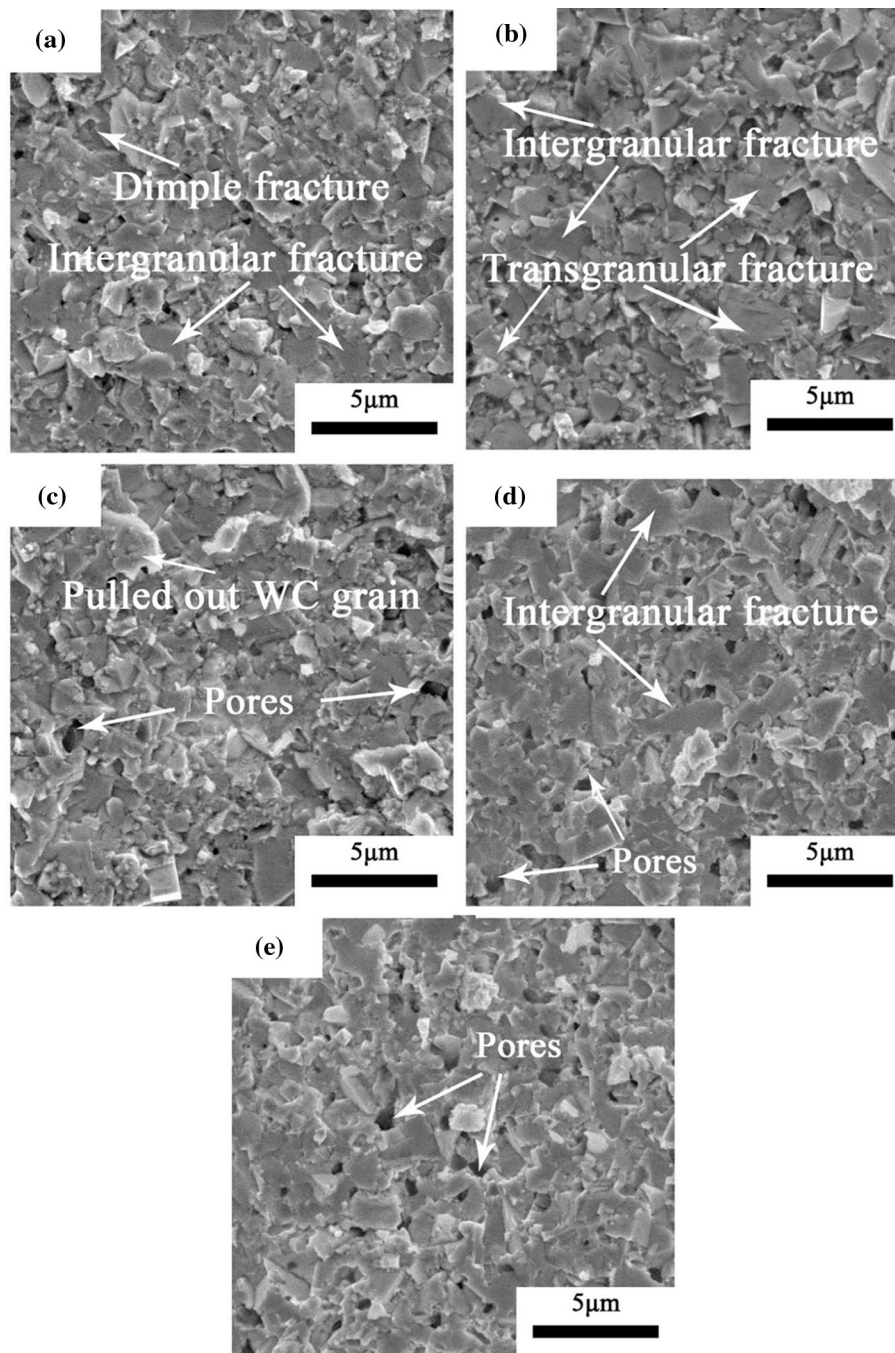


**Fig. 13** Fracture morphology images of WC-10 wt.%CoCrFeNiAl<sub>x</sub> cemented carbides: (a)  $x = 0$ ; (b)  $x = 0.25$ ; (c)  $x = 0.5$ ; (d)  $x = 0.75$ ; and (e)  $x = 1.0$

### Acknowledgments

This work was supported by the Shandong Province science and technology smes innovation ability improvement project (Grant No. 2023TSGC0531)

### Author Contributions

WZ was contributed to investigation, writing—original draft preparation. ZS was contributed to investigation, writing—original draft preparation. ZW was contributed to project administration, writing—review and editing. ZS was contributed to supervision.

YC was contributed to investigation. All authors have seen and approved the manuscript.

### Data Availability

Data will be made available on request.

### Conflict of interest

The authors declare that they have no known competing financial interests or personal relationships that could have appeared to influence the work reported in this paper.

## References

1. K.W. Kim, A.B. Kale, Y.H. Cho, S.H. Park, and K.A. Lee, Microstructural and Wear Properties of WC-12Co Cemented Carbide Fabricated by Direct Energy Deposition, *Wear*, 2023 <https://doi.org/10.1016/j.wear.2023.204653>
2. S. Yu, F. Min, G. Ying, J.G. Noudem, S. Liu, and J. Zhang, The Grain Growth and Boundary Evolution of Extra-Coarse-Grained Cemented Carbides by Pressureless Sintering of Ball-Milling-Mixed WC with Co at Different Temperature, *Mater Charact*, 2021, **180**, p 111386.
3. Y.X. Wen, M.C. Zhang, and Y. Zhang, The Effect of Binder Phase Content on WC-AlCoCrFeNiTi<sub>0.2</sub> High Entropy Cemented Carbides Microstructure and Mechanical Properties, *Res. Appl. Mater. Sci.*, 2022, **4**, p 10–15.
4. M. Tarraste, J. Kübarsepp, K. Juhani, A. Mere, M. Kolnes, M. Viljus, and B. Maaten, Ferritic Chromium Steel as Binder Metal for WC Cemented Carbides, *Int. J. Refract. Met. Hard Mater.*, 2018, **73**, p 183–191.
5. Z. Zhao, K. Wang, Y. Hu, and Y. Dong, Microstructure and Properties of Coarse WC-10CoCrFeMnNi Cemented Carbide by Mechanical Alloying and Hot Pressing Sintering, *Mater. Today Commun.*, 2023, **37**, p 107137.
6. Q. Yang, J. Yang, Y. Wen, Q. Zhang, L. Chen, and H. Chen, A Novel Route for the Synthesis of Ultrafine WC-15 wt %Co Cemented Carbides, *J. Alloy. Compd.*, 2018, **748**, p 577–582.
7. W. Luo, Y. Liu, X. Liu, and Z. Zhou, Oxidation Behavior of Ultrafine WC-based Cemented Carbides with AlCoCrCuFeNi High-Entropy Alloy Binders, *Ceram. Int.*, 2021, **47**(6), p 8498–8509.
8. M. Ghanbariha, M. Farvizi, T. Ebadzadeh, A. Alizadeh Samiyan, and H.S. Kim, AlCoCrFeNi-NiTi High Entropy Alloy Composites: Microstructure and Wear Performance, *Mater. Today Commun.*, 2022, **32**, p 103952.
9. S. Zhu, J. Hui, X. Sun, H. Bin, and D. Weiwei, Effect of Phase Transformation of CoCrFeNiAl High-Entropy Alloy on Mechanical Properties of WC-CoCrFeNiAl Composites, *Ceram. Int.*, 2023, **49**, p 32388–32398.
10. D. Dong, X. Xiang, B. Huang, H. Xiong, L. Zhang, K. Shi, and J. Liao, Microstructure and Properties of WC-Co/CrMnFeCoNi Composite Cemented Carbides, *Vacuum*, 2020, **179**, p 109571.
11. M.M. Garlapati, M. Vaidya, A. Karati, S. Mishra, R. Bhattacharya, and B.S. Murty, Influence of Al Content on Thermal Stability of Nanocrystalline Al<sub>x</sub>CoCrCuFeNi High Entropy Alloys at Low and Intermediate Temperatures, *Adv. Powder Technol.*, 2020, **31**, p 1985–1993.
12. P.F. Zhou, D.H. Xiao, and T.C. Yuan, Comparison Between Ultrafine-Grained WC-Co and WC-HEA-Cemented Carbides, *Powder Metall.*, 2017, **60**(1), p 1–6.
13. C.S. Chen, C.C. Yang, H.Y. Chai, J.W. Yeh, and J.L.H. Chau, Novel Cermet Material of WC/Multi-Element Alloy, *Int. J. Refract. Met. Hard Mater.*, 2014, **43**, p 200–204.
14. Y.Y. Liu, Z. Chen, J.C. Shi, Z.Y. Wang, and J.Y. Zhang, The Effect of Al Content on Microstructures and Comprehensive Properties in Al<sub>x</sub>CoCrCuFeNi High Entropy Alloys, *Vacuum*, 2019, **161**, p 143–149.
15. K. Lu, H. Wang, S. Fan, Y. Liu, N. Guo, F. Yin, and J. Zhu, Effect of Al Elements on the Microstructure and Properties of CoCrNiCuMoAl<sub>x</sub> High-Entropy Alloys, *Jom*, 2022, **74**(11), p 4138–4145.
16. L. Chen, D. Yi, B. Wang, H. Liu, C. Wu, X. Huang, H. Li, and Y. Gao, The Selective Oxidation Behaviour of WC-Co Cemented Carbides During the Early Oxidation Stage, *Corros. Sci.*, 2015, **94**, p 1–5.
17. W.D. Schubert, H. Neumeister, G. Kinger, and B. Lux, Hardness to Toughness Relationship of Fine-Grained WC-Co Hardmetals, *Int. J. Refract. Met. Hard Mater.*, 1998, **16**, p 133–142.
18. B. Roebuck and W. Coles, Mechanical Test Discriminability for WC Hardmetals, *Int. J. Refract. Met. Hard Mater.*, 1992, **11**, p 127–136.
19. G. Xu, W. Liu, C. Yi, K. Zheng, M. Yi, J. Zhang, G. Xiao, Z. Chen, and C. Xu, Formation of Solid Solution Structures in (Ti, W, Ta, Mo)(C, N) Cermet Via Spark Plasma Sintering, *Int. J. Refract. Met. Hard Mater.*, 2023, **113**, p 106218.
20. T. Borkar, B. Gwalani, D. Choudhuri, C.V. Mikler, C.J. Yannetta, X. Chen, R.V. Ramanujan, M.J. Styles, M.A. Gibson, and R. Banerjee, A Combinatorial Assessment of Al<sub>x</sub>CrCuFeNi<sub>2</sub> (0 < x < 1.5) Complex Concentrated Alloys: Microstructure Microhardness and Magnetic Properties, *Acta Mater.*, 2016, **116**, p 63–76.
21. R. Sriharitha, B.S. Murty, and R.S. Kottada, Phase formation in mechanically alloyed Al<sub>x</sub>CoCrCuFeNi (x=0.45, 1, 2.5, 5mol) high entropy alloys, *Intermetallics*, 2013, **32**, p 119–126.
22. R. de O. Calderon, C.G. Mayer, and H. Danninger, Fundamentals of Sintering: Liquid Phase Sintering, Eds. by G. Francisca Caballero, Encyclopedia of Materials: Met. Alloy., P 481–492 (2022)
23. X. Wang, D. Zhou, and P. Xu, The WC-Co/Fe-Ni Interface: EFFECT of Holding Time on the Microstructure, Grain Size and Grain Growth Mechanism, *Ceram. Int.*, 2019, **45**, p 23320–23327.
24. W.Y. Luo, Y. Liu, and J. Shen, Effects of Binders on the Microstructures and Mechanical Properties of Ultrafine WC-10%Al<sub>x</sub>CoCrCuFeNi Composites by Spark Plasma Sintering, *J. Alloy. Compd.*, 2019, **791**, p 540–549.
25. J. Huang, J. He, Z. Li, L. Shen, L. Chen, F. Chang, P. Dai, and Q. Tang, Effect of WC Addition on Microstructure and Properties of Powder Metallurgy CoCrNi Medium Entropy Alloy, *Mater. Today Commun.*, 2023, **36**, p 106435.
26. X. Li, L. Wang, Y. Liu, and J. Ye, Enhanced High Temperature Mechanical Properties of WC-Co Cemented Carbides by VC Addition, *Int. J. Refract. Met. Hard Mater.*, 2023, **116**, p 106355.
27. X. Chen, Y. Liu, J. Ye, L. Wang, and D. Li, Effect of Rapid Cooling on Microstructure and Properties of Nanocrystalline WC-9%Co-Cr<sub>3</sub>C<sub>2</sub>-VC Cemented Carbide, *Int. J. Refract. Met. Hard Mater.*, 2022, **109**, p 105961.
28. W.Y. Luo, Y. Liu, and C. Tu, Wetting Behaviors and Interfacial Characteristics of Molten Al<sub>x</sub>CoCrCuFeNi High-Entropy Alloys on a WC Substrate, *J. Mater. Sci. Technol.*, 2021, **78**, p 192–201.
29. M.H. Mohammad-Ebrahimi, A. Zarei-Hanzaki, H.R. Abedi, S.M. Vakili, and C.K. Soundararajan, Decelerated Grain Growth Kinetic and Effectiveness of Hall-Petch Relationship in a Cold-Rolled Non-Equiatomic High Entropy Alloy, *J. Alloy. Compd.*, 2021, **874**, p 159849.
30. R. Furushima, K. Katou, S. Nakao, Z.M. Sun, K. Shimojima, H. Hosokawa, and A. Matsumoto, Relationship Between Hardness and Fracture Toughness in WC-FeAl Composites Fabricated by Pulse Current Sintering Technique, *Int. J. Refract. Met. Hard Mater.*, 2014, **42**, p 42–46.
31. D. Kumar, O. Maulik, S. Kumar, Y.V.S.S. Prasad, and V. Kumar, Phase and Thermal Study of Equiatomic AlCuCrFeMnW High Entropy Alloy Processed Via Spark Plasma Sintering, *Mat. Chem. Phys.*, 2018, **210**, p 71–77.
32. C.J. Tong, M.R. Chen, and J.W. Yeh, Mechanical Performance of the Al<sub>x</sub>CoCrCuFeNi High-Entropy Alloy System with Multiprincipal Elements, *Metall. Mater. Trans.*, 2005, **36**, p 1263.
33. Z. Fu and R. Koc, Ultrafine TiB<sub>2</sub>-TiNiFeCrCoAl High-Entropy Alloy Composite with Enhanced Mechanical Properties, *Mater. Sci. Eng.*, 2017, **702**, p 184–188.
34. T. Li, Q. Li, J.Y.H. Fuh, P.C. Yu, L. Lu, and C.C. Wu, Effects of AGG on Fracture Toughness of Tungsten Carbide, *Mater. Sci. Eng.*, 2007, **445–446**, p 587–592.
35. T. Bai and T. Xie, Fabrication and Mechanical Properties of WC-Al<sub>2</sub>O<sub>3</sub> Cemented Carbide Reinforced by CNTs, *Mat. Chem. Phys.*, 2017, **201**, p 113–119.
36. L.S. Sigl, P.A. Mataga, B.J. Dalgleish, R.M. McMeeking, and A.G. Evans, On the Toughness of Brittle Materials Reinforced with a Ductile Phase, *Acta Metall.*, 1988, **36**, p 945–953.
37. J.M. Tarragó, D. Coureaux, Y. Torres, E. Jiménez-Piqué, L. Schneider, J. Fair, and L. Llanes, Strength and Reliability of WC-Co Cemented Carbides: Understanding Microstructural Effects on the Basis of R-Curve Behavior and Fractography, *Int. J. Refract. Met. Hard Mater.*, 2018, **71**, p 221–226.

**Publisher's Note** Springer Nature remains neutral with regard to jurisdictional claims in published maps and institutional affiliations.

Springer Nature or its licensor (e.g. a society or other partner) holds exclusive rights to this article under a publishing agreement with the author(s) or other rightsholder(s); author self-archiving of the accepted manuscript version of this article is solely governed by the terms of such publishing agreement and applicable law.